Advancement of the Oxidized State of an As-Cast Low-Mn, High-Cr Cantor's Alloy in Natural Air at 1000 °C

Lyna Amrouche, Patrice Berthod

▶ **To cite this version:**

Lyna Amrouche, Patrice Berthod. Advancement of the Oxidized State of an As-Cast Low-Mn, High-Cr Cantor's Alloy in Natural Air at 1000 °C. Corrosion and Materials Degradation, 2024, 5, pp.601 - 614. 10.3390/cmd5040028 . hal-04824844

HAL Id: hal-04824844
https://hal.science/hal-04824844v1

Submitted on 7 Dec 2024

HAL is a multi-disciplinary open access archive for the deposit and dissemination of scientific research documents, whether they are published or not. The documents may come from teaching and research institutions in France or abroad, or from public or private research centers.

L'archive ouverte pluridisciplinaire **HAL**, est destinée au dépôt et à la diffusion de documents scientifiques de niveau recherche, publiés ou non, émanant des établissements d'enseignement et de recherche français ou étrangers, des laboratoires publics ou privés.

Distributed under a Creative Commons Attribution 4.0 International License

corrosion and materials degradation

MDPI

Article

Advancement of the Oxidized State of an As-Cast Low-Mn, High-Cr Cantor's Alloy in Natural Air at 1000 °C

Lyna Amrouche [1] and Patrice Berthod [2,*]

[1] Faculté des Sciences et Technologies, Université de Lorraine, 54000 Vandoeuvre–lès-Nancy, France; lyna.amrouche2@etu.univ-lorraine.fr
[2] CNRS, Institut Jean Lamour, Université de Lorraine, 54000 Nancy, France
* Correspondence: patrice.berthod@univ-lorraine.fr; Tel.: +33-3-72-74-27-29

Abstract: In order to discover how the multiple oxides observed in the final external scales after long exposure of a low-Mn, high-Cr Cantor's alloy to hot air were formed, oxidation tests in a furnace were performed for seven different durations. Metallographic characterization was carried out concerning the oxidation products obtained after each test duration. The different oxides did not appear one after the other, but simultaneously, early on in the exposure to hot air and after. They all thickened progressively and the chemical composition of each also evolved with time, more or less. Globally, the innermost oxide is almost entirely chromia, much richer in Cr than in Mn, while the outermost one contains principally Mn. The interrupted tests also allowed specifying the mass gain kinetic, which is parabolic and twice as fast as a chromia-forming alloy. Despite the lowered content in Mn, manganese still plays an important role in the oxidation phenomenon, starting very early.

Keywords: modified Cantor alloy; manganese; chromium; high temperature; oxidation progress

check for updates

Citation: Amrouche, L.; Berthod, P. Advancement of the Oxidized State of an As-Cast Low-Mn, High-Cr Cantor's Alloy in Natural Air at 1000 °C. *Corros. Mater. Degrad.* **2024**, *5*, 601–614. https://doi.org/10.3390/cmd5040028

Academic Editors: Angeliki G. Lekatou and Markus Valtiner

Received: 4 October 2024
Revised: 26 November 2024
Accepted: 28 November 2024
Published: 2 December 2024

Copyright: © 2024 by the authors. Licensee MDPI, Basel, Switzerland. This article is an open access article distributed under the terms and conditions of the Creative Commons Attribution (CC BY) license (https://creativecommons.org/licenses/by/4.0/).

1. Introduction

From many decades, cobalt, nickel and iron have been the most common elements serving as a base for superalloys [1,2]. The first two cited ones are increasingly being considered as critical or strategic [3,4]. Decreasing their contents in a superalloy, by a limited replacement with elements such as iron or manganese, may be a solution to becoming less dependent on Co and Ni. Such changes in the chemical composition, in the presence of chromium, to combat both hot oxidation and corrosion [5,6] through the development of a covering chromia scale (chromia-forming superalloys) may lead to the composition principle of the Cantor alloy [7]. This equimolar Co-Ni-Fe-Mn-Cr alloy belongs to a family of quinary alloys [8–10] and is one of the most well-known high- entropy alloy (HEA) systems [11].

In order to succeed in replacing superalloys with new ones that are less dependent on Co and Ni thanks to the presence of Fe and Mn, the properties of such new alloys at high temperatures must be strong enough. It is thus important to know their properties to verify if this is indeed the case. Many properties of the HEAs conceived on Co-Ni-Fe-Mn-Cr systems have been extensively studied at other temperatures. Such studies revealed, for example, their interesting behaviors at cryogenic to moderate temperatures. Unfortunately, reported observations concerning their properties at temperatures up to 1000 °C are not numerous to date, notably concerning their behavior under oxidation [12–15]. Concerning the mechanical properties, one may mention recent successful attempts to improve high-temperature strength by adding MC eutectic carbides to an equimolar base [16]. The behavior under oxidation of these MC-reinforced Cantor's alloys at 1000 °C and beyond was explored [17]: this revealed severe problems of oxidation resistance at such high temperatures, attributed to particular roles of chromium and manganese together. Indeed, despite the presence of about 25 at.% Cr, the tested alloys, with or without MC carbides, oxidized rapidly. Many kinds of oxides—primarily involving Mn and Cr in various proportions and sometimes other elements, too—formed

externally. In order to observe how these oxides formed, a series of samples of Cantor's alloys (equimolar in Co, Ni, Fe, Mn and Cr) were exposed to air at 1000 °C for several durations (up to 62 h), which led to a better understanding of the successive steps of the oxidation progress [18]. Some Mn-impoverished, Cr-enriched versions of these alloys (reinforced by MC carbides or not) were tested in oxidation at 1000 °C with mass variation continuous follow-up using a thermo-balance [19]. This revealed that decreasing Mn and increasing Cr led to a significantly improved oxidation behavior in terms of mass gain kinetic. The post-mortem characterization of the oxidized thermogravimetry samples showed that the oxidation products formed around these samples were different by comparison with the equimolar version. This also showed that, here too, the oxide scales were constituted of various types of oxides in which again Mn seemingly played an important role.

To better understand how and in which order the different observed oxides formed, the same method of oxidation as described above was applied in the present work for the equimolar alloy [18], this time for an Mn-decreased, Cr-increased version. The $CoNiFeMn_{0.5}Cr_{1.5}$ alloy was oxidized for several durations at 1000 °C and the progression of oxidation was observed by analyzing the step-by-step development of the complex oxide scale.

2. Materials and Methods

A 40 g ingot was first synthesized by fusion using high-frequency induction (50 kW CELES furnace, operating parameters: 100 kHz, 3 to 5 A, up to 5 kV) in a pure argon atmosphere. The initial charge contained small balls, flakes or rods of pure Co, Ni, Fe, Mn and Cr (Alfa Aesar, purity > 99.9%). During melting and the 10 min stage at maximal power, the liquid alloy became homogenized and the oxides initially present in the pure elements (notably Mn) were expelled by the electromagnetic stirring. No homogenization treatment was applied after casting to allow the eventual segregations developed during solidification in the oxidation phenomena, and thus place the alloy in the most severe oxidation situation. The obtained chemical compositions were controlled on specimens specially prepared by cutting, embedding and polishing using X-ray diffraction (XRD) and electron microscopy. In the first case, a Bruker D8 Advance was used (Cu Kα radiation) and the spectral exploitation was performed using the EVA software (V5.0 version) and an adequate database. In the latter case, a JEOL 6010LA scanning electron microscope (SEM) (Tokyo, Japan) and its energy dispersion spectrometer (EDS) were used. A series of parallelepipeds, obtained by cutting, were ground using #1200-grit SiC paper. Their edges and corners were smoothed with the same paper to avoid possible local overoxidation. After accurate measurement of their dimensions using a caliper (precision: +/−0.01 mm) and after weighing with a micro-balance (precision: +/− 0.1 mg), each sample was placed in a nacelle (made of a refractory inert material) which was introduced in the hottest zone of a tubular resistive furnace (Carbolite).

After 1.5 h, 3 h, 6 h, 9 h, 15 h, 24 h or 62 h, the nacelle was promptly removed from the furnace. After naturally cooling down to ambient temperature, the oxidized alloy was carefully handled for the next operations. After a second weighing with the micro-balance, the oxidized sample was observed with the SEM (secondary electrons mode (SE) and back scattered electrons mode (BSE)) as well as subjected to EDS spot analysis and elemental mapping. Later, it was embedded in a resin rigidifying at ambient temperature, then transversally cut and grinded/polished. The obtained mirror-like cross-section allowed for observing the external and internal oxides and performing EDS spot analyses and elemental mapping on the oxides and the subsurface.

3. Results

3.1. Characteristics of the Alloy Subject of the Study

After solidification and cooling down to laboratory temperature, a part of the ingot was metallographically prepared and characterized. XRD demonstrated that the alloy is single-phased (FCC). The diffractogram indicating the presence of the FCC single phase can be seen in Figure 1. This was seen again using an SEM and its EDS spectrometer. Its

chemical composition, as determined by several EDS full frame analyses, is close to the target one (Table 1).

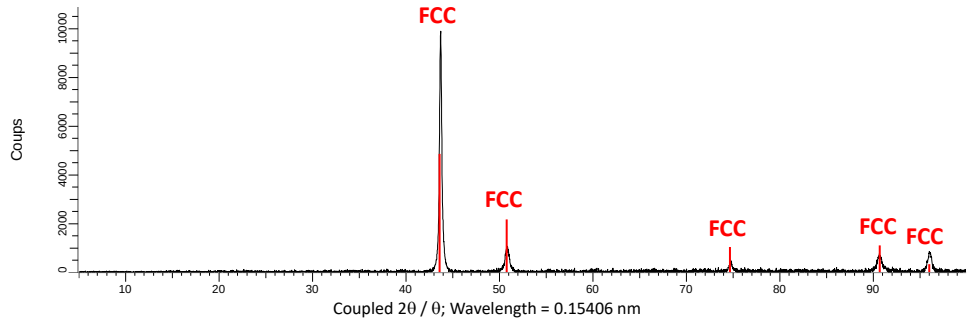

Figure 1. Diffractogram acquired on the as-cast alloy elaborated for the study.

Table 1. Chemical compositions of the alloy elaborated for the study (determined from five ×250 full-frame EDS analyses per alloy); weight contents in all elements and the corresponding atomic contents.

Content in…		Co	Ni	Fe	Mn	Cr
wt.%	Average	20.0	20.5	19.8	8.3	31.3
wt.%	Std dev	0.1	0.3	0.2	0.5	0.4
at.%		18.9	19.4	19.7	8.4	33.5

3.2. Mass Evolution with Time

All samples were accurately weighed before and after exposure to hot air, allowing quantification of the mass gain due to oxidation. The seven obtained mass gain values (after 1.5 h, 3 h, 6 h, 9 h, 15 h, 24 h and 62 h of oxidation) are plotted versus time (A) and versus the square root of time (B) in Figure 2. Versus time, the mass gain $\frac{\Delta m}{S}(t)$ seems parabolic, and thus it obeys Wagner's law (Equation (1)).

$$\frac{\Delta m}{S}(t) = \sqrt{2 \times Kp} \times \sqrt{t} \quad (1)$$

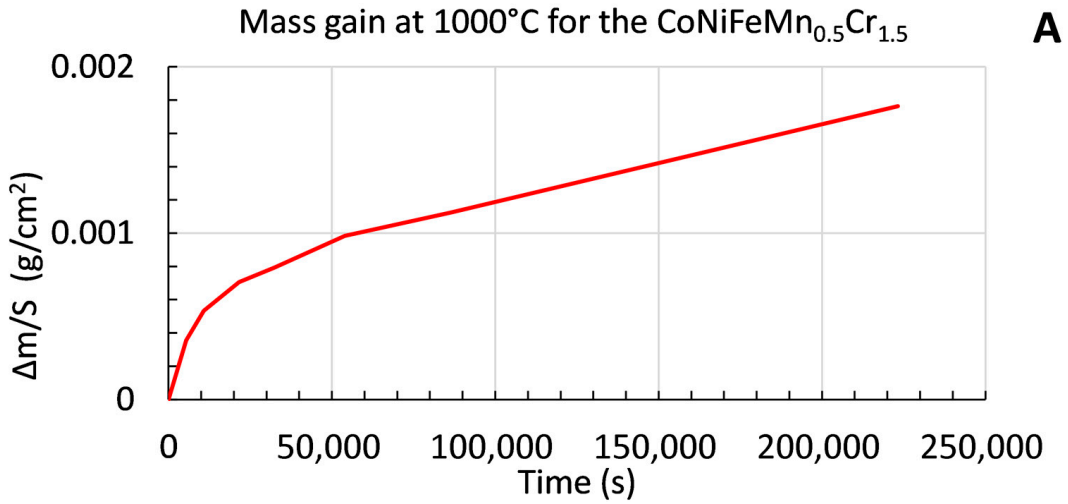

Figure 2. *Cont.*

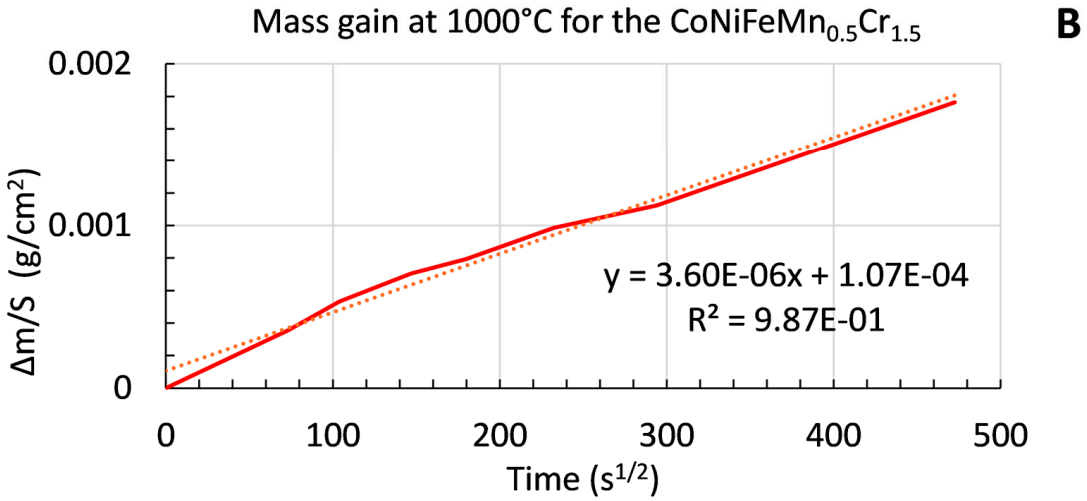

Figure 2. Progress in mass gain per surface unit area due to oxidation versus time (**A**) and versus the square root of time (**B**).

The slope of the rather straight line obtained when plotting against the square root of time (bottom) leads to a kinetic parabolic constant $Kp = 6.5 \times 10^{-12}$ g^2 cm^{-4} s^{-1}.

3.3. General Appearance of the Oxidized Surfaces

The outermost surfaces of the external oxide scales were examined and analyzed prior to cross-sectional metallographic preparation. Low-magnification observation using SEM in SE mode (Figure 3) allows observation of how the morphology of the outermost oxide evolves with time at 1000 °C. After only 1.5 h of exposure, the alloy is entirely covered by oxides. The scale is composed of coarse oxides appearing as filaments in relief over a finer oxide structure. The double population of outermost coarse oxides and inner fine oxides is still present after 3 h of exposure, with the coarse oxides appearing less numerous and more coalesced. Later (15 h), the external roughness of the scale is uniformly fine before new coarse oxides appear (24 h, 62 h).

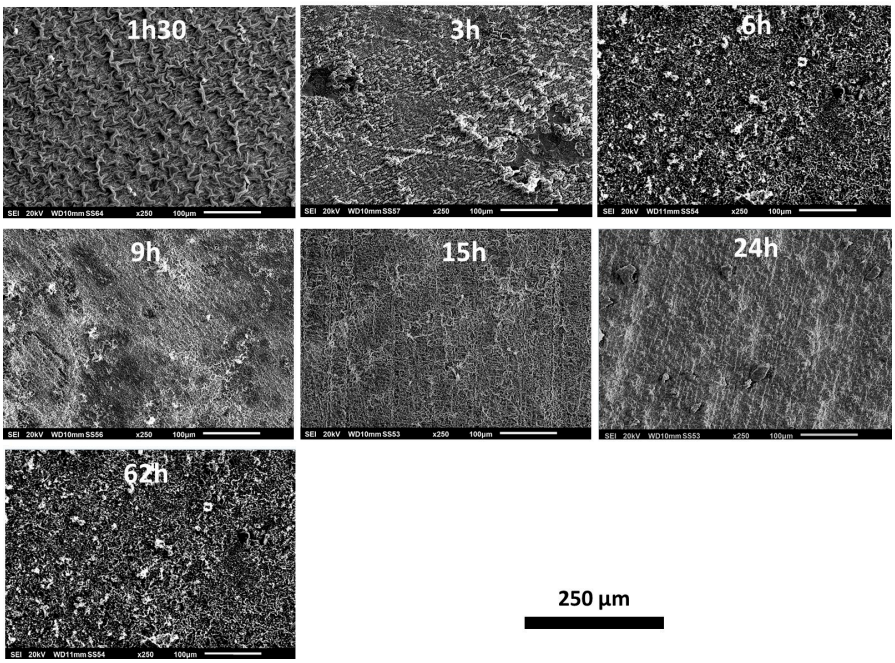

Figure 3. General appearance of the oxidized scales developed over the seven samples (low-magnification SEM micrographs, SE imaging mode).

3.4. Average Composition of the External Scales

The outermost average compositions of the oxide scale assessed by EDS full-frame analysis at ×1000 magnification (Figure 4) suggests that the external oxides are complex, involving all the elements present in the alloy. Among them, chromium is the most present oxidized element after 1.5 h. For the durations between 3 h and 15 h, Mn is as present as Cr in the oxides. After 24 h and 62 h of oxidation, Mn is the metal which is the most present as an oxide. Fe and Co are also affected by oxidation regardless of the duration, but to a much lesser extent than Mn and Cr.

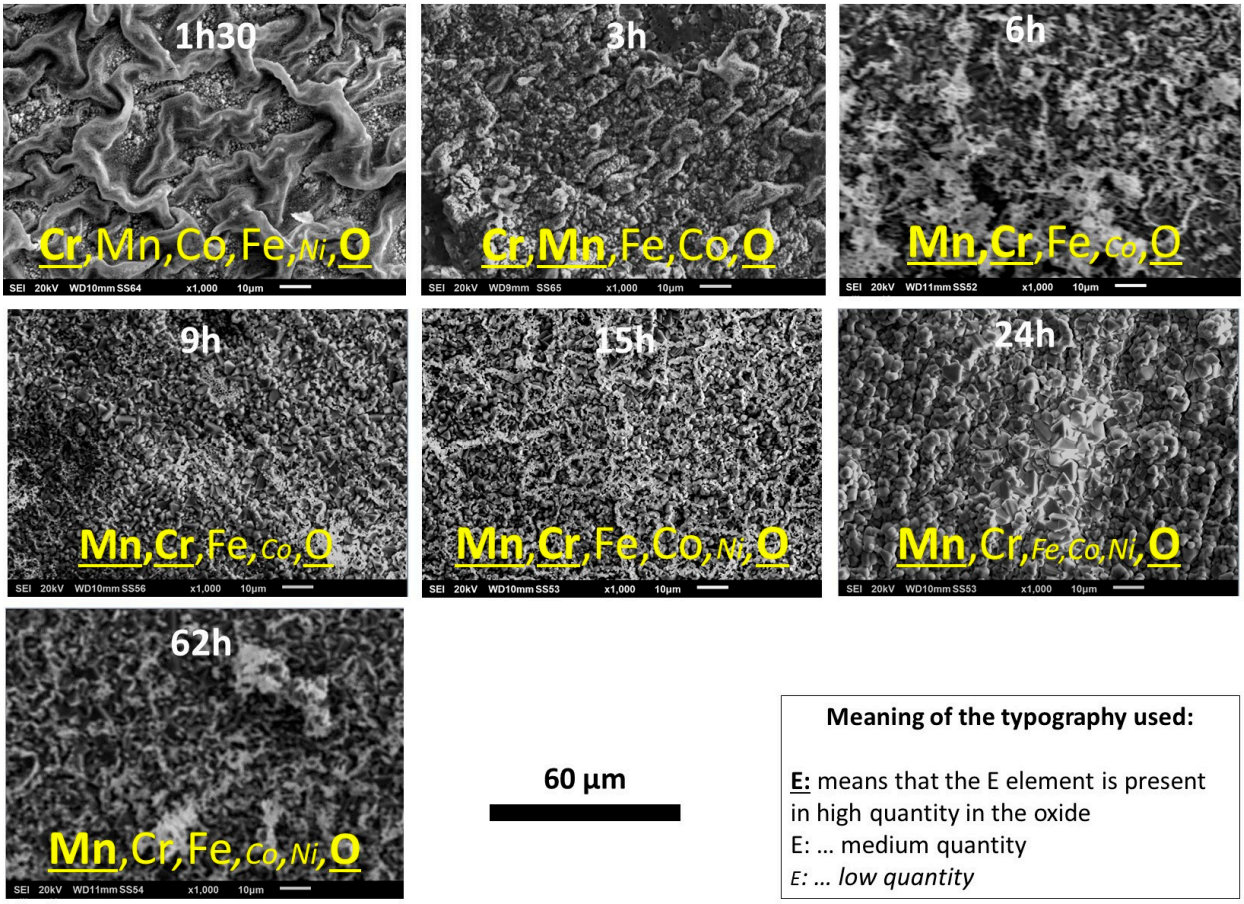

Figure 4. Details of the oxidized oxide scales developed over the seven samples (high-magnification SEM micrographs, SE imaging mode).

3.5. Elemental Distribution on the Outermost Face of the Oxide Scale

EDS elemental mapping was performed on the external face of the oxide scales using a 20 kV acceleration voltage. Selected results are presented in Figure 5 for 1.5 h, in Figure 6 for 3 h, in Figure 7 for 15 h and in Figure 8 for 24 h.

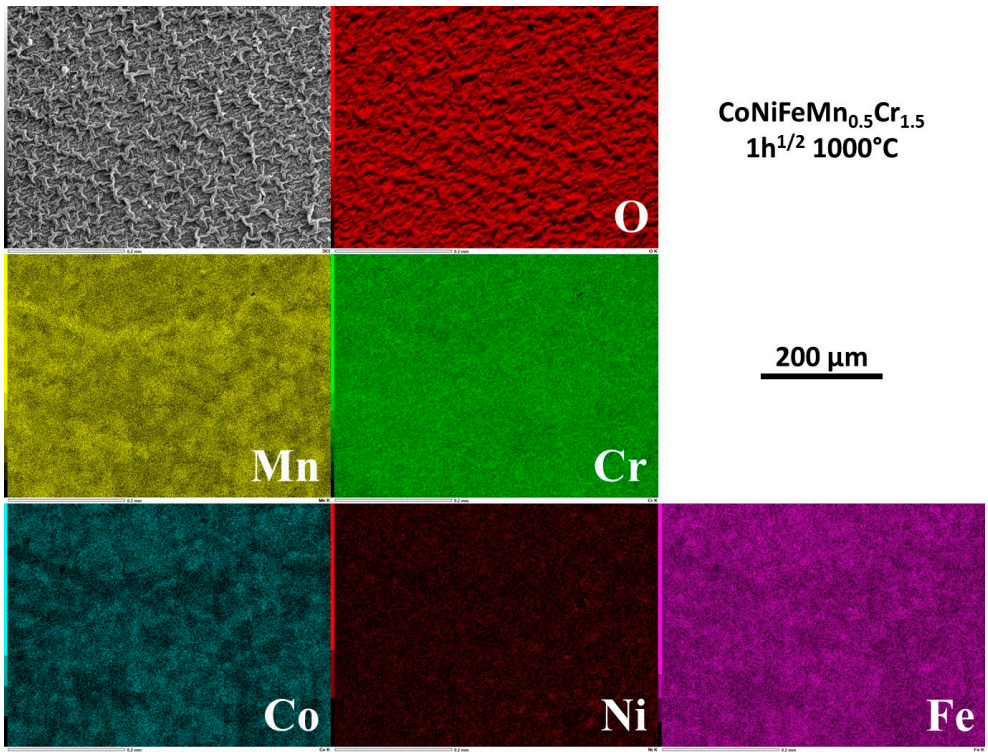

Figure 5. Elemental distribution detected by EDS on the outermost side of the external oxide scale formed after 1.5 h of exposure.

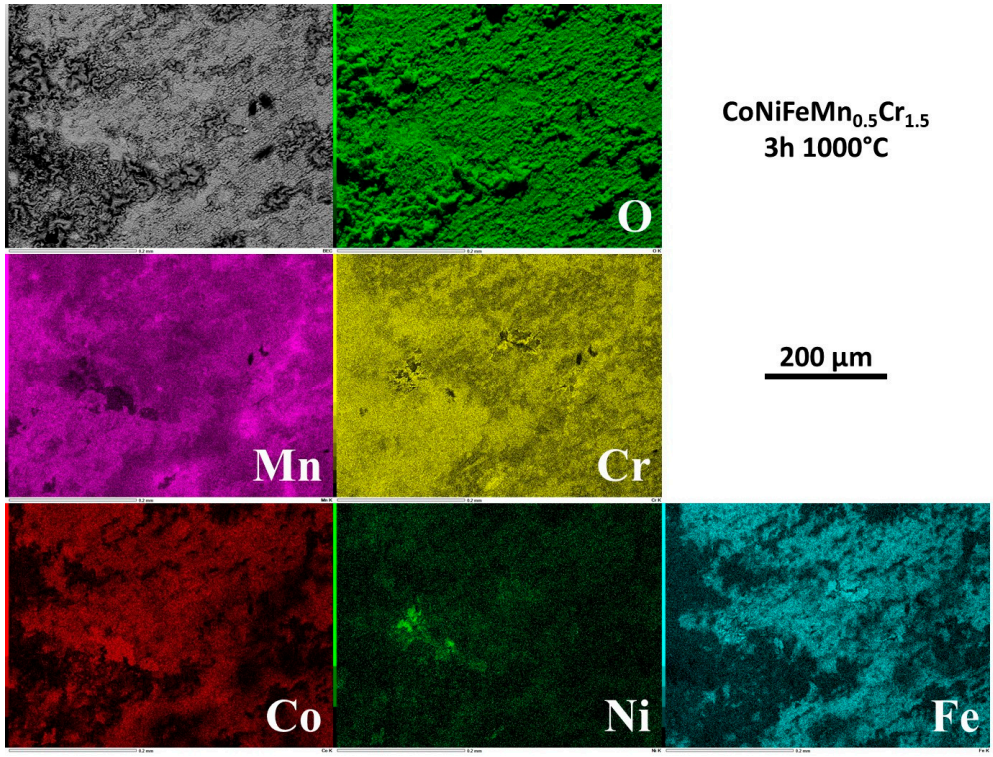

Figure 6. Elemental distribution detected by EDS on the outermost side of the external oxide scale formed after 3 h of exposure.

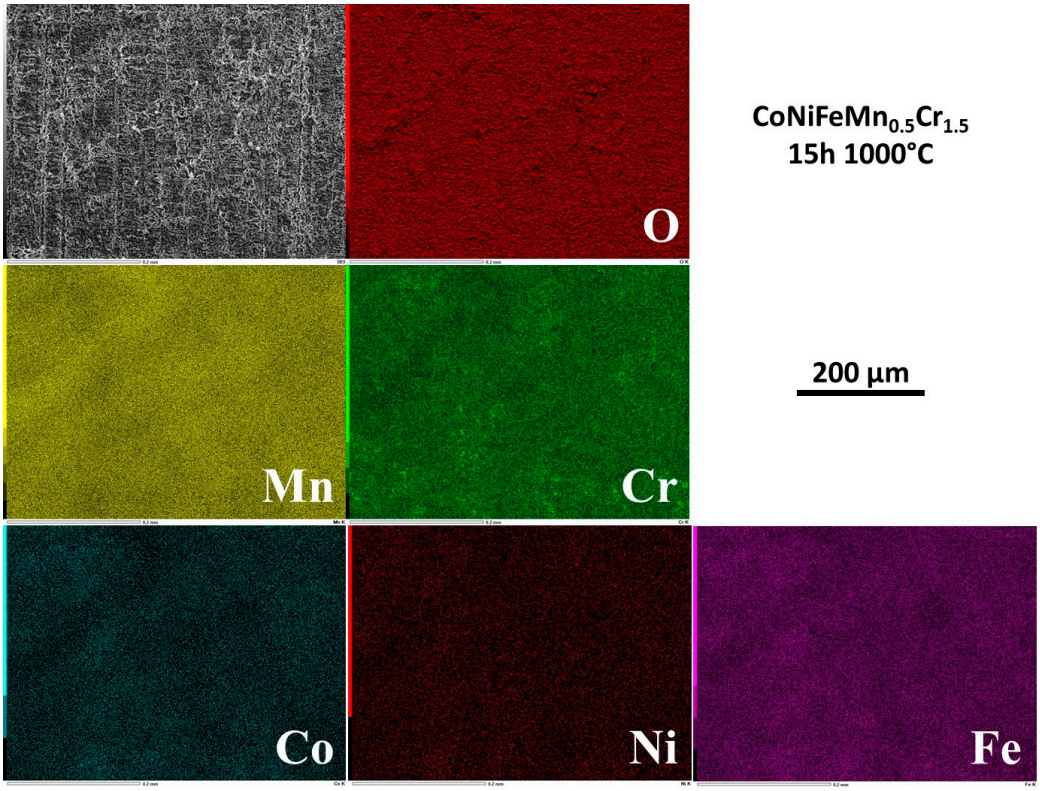

Figure 7. Elemental distribution detected by EDS on the outermost side of the external oxide scale formed after 15 h of exposure.

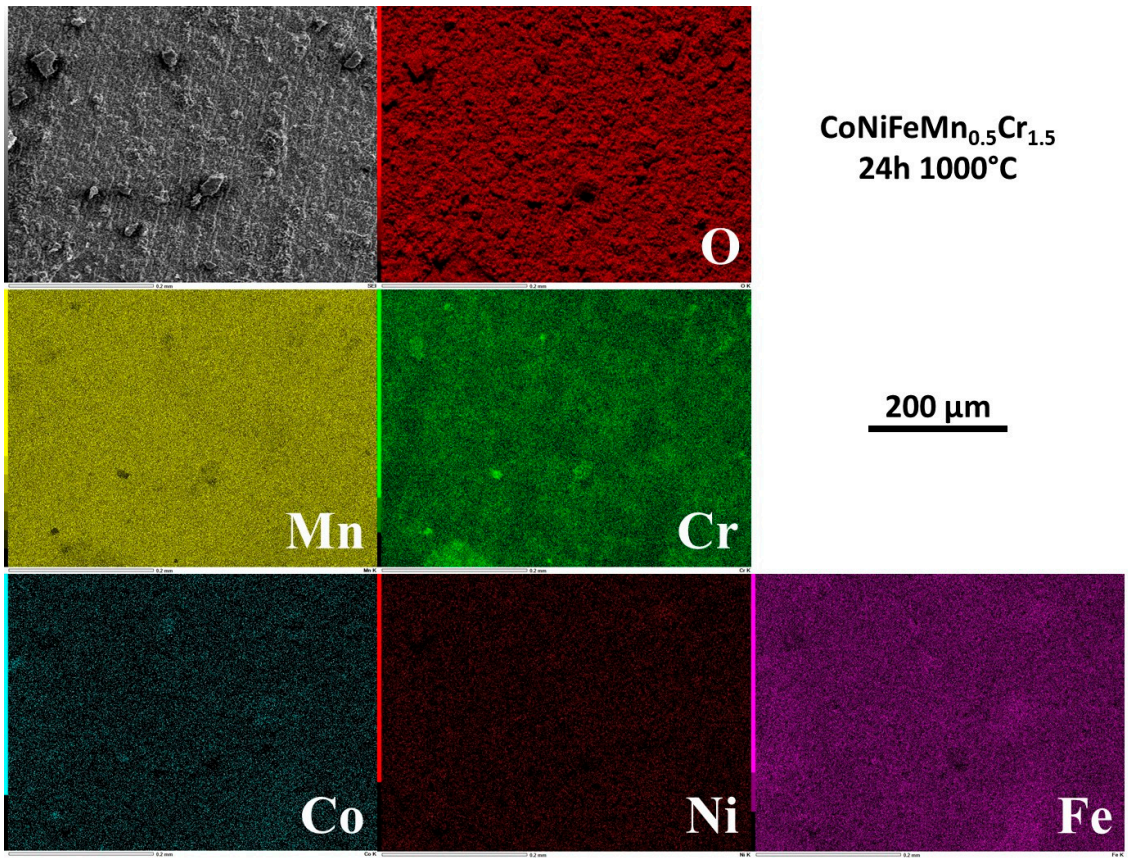

Figure 8. Elemental distribution detected by EDS on the outermost side of the external oxide scale formed after 24 h of exposure.

After 1.5 h the metals are heterogeneously distributed in the external oxide scale. There are zones rich in Mn and Cr, and other zones are made up of a complex oxide involving Cr, Fe, Co and a small quantity of Ni (Figure 5). At 3 h (Figure 6), Mn and Cr are obviously involved in coarse oxides covering only parts of the surface, which is elsewhere seemingly covered by thinner oxides containing more Fe and Co. Rare small parts of the surface present manganese oxides and other parts have high concentrations of Ni, Co and Fe, suggesting that the alloy is almost denuded locally. After 15 h of exposure and longer (Figures 7 and 8), the chemical composition of the external face of the scales is more homogeneous. Manganese (homogeneous) and chromium (more heterogeneous) are the most present elements. The presence of Co and Fe is to be noticed here and they are in combination with local high levels of Cr, in correspondence with the coarsest oxides present in the relief.

One must note that these EDS elemental maps were acquired using a rather high acceleration voltage (20kV), and it is possible that the underlying alloy influenced the results in addition to the oxide scale, especially for the thinner oxide scales. Consequently, the observations presented above (particularly the chemical heterogeneity) need to be verified by Grazing Incidence X-Ray Diffraction (GIXRD) or EDS mapping at voltages lower than 20 kV when analyzing the oxide scale only.

3.6. Cross-Sectional Observation and Characterization of Oxide Scale and Subsurface

After cutting and surface preparation by grinding and polishing, the external oxide scale and the subsurface can be observed in cross-section (Figure 9). It was not possible to perform accurate EDS spot analysis in the too-thin scale existing after 1.5 h. Longer-exposure EDS spot analyses allowed acquiring data useful for the identification of the different oxides present: an outermost scale rich in Mn and Cr together (also with a minor presence of the three other metals) and an innermost scale of oxides of mainly Cr but also of Mn, with the M_2O_3 stoichiometry of chromia. The particularly high involvement of Cr and Mn in the oxidation phenomena led to significant subsurface impoverishment in these two elements. Spot analyses were performed in the part of the alloy that is very close to its interface with the oxide scale. The results showed that the Cr and Mn contents are decreased by comparison to the initial values (about 5 wt.% less for chromium and from 5 to 8 wt.% less for manganese).

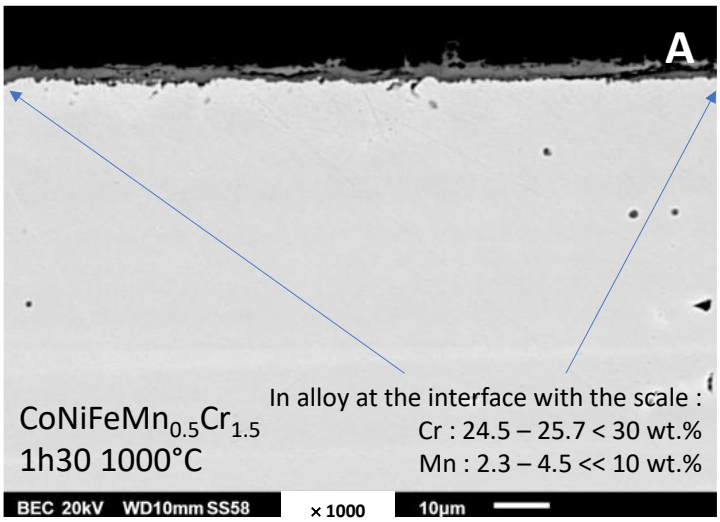

Figure 9. *Cont.*

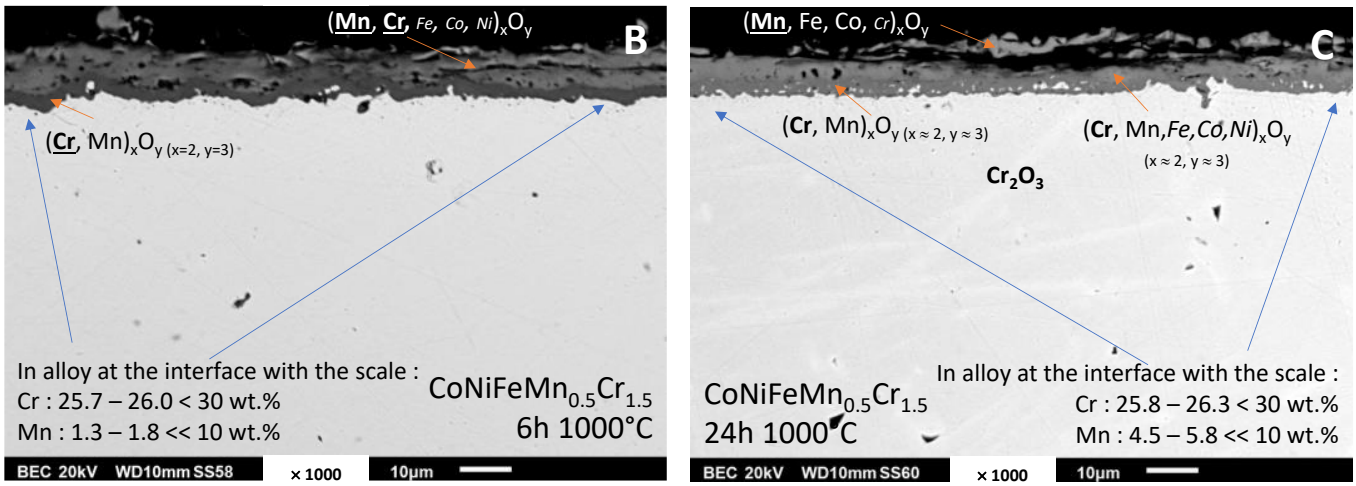

Figure 9. Cross-sectional view of the oxide scale and the subsurface of three of the oxidized samples (**A**: 1.5 h; **B**: 6 h; and **C**: 24 h); EDS spot analysis results obtained from the different oxides; chemical composition in alloy close to the interface with the scale.

3.7. EDS Elemental Mapping over the Zones Affected by Oxidation

The repartition of the elements involved by oxidation was also investigated by EDS elemental mapping. Four examples of elemental maps are given in Figure 10 for 1.5 h, Figure 11 for 6 h, Figure 12 for 24 h and Figure 13 for 62 h. This type of EDS result is qualitative but provides a better understanding of how the oxide scale formed and how it progressed with time. One can see that all the elements present in the alloy took part in oxidation, in various proportions, as soon as the sample started to oxidize. After only 1.5 h (Figure 10), the oxide scale was already continuous all the way around the sample and constituted superposed thin scales. From the outer side of the scale to the interface with the alloy, one encounters 1) an outermost layer—plastically deformed during cooling at the end of the test—made of oxides mainly composed of manganese but with the presence of Cr as a minor species; 2) a middle layer containing all metals from the alloy (except Cr, curiously); and 3) an internal layer of oxides composed mainly of mainly Cr but also containing Mn. A little later (6 h, Figure 11), the scale has logically become thicker. Fe is present in the outermost $Mn(Fe)_xO_y$ layer, the middle layer is mainly an Fe oxide (with presence of Cr and Co) and the innermost layer is still a $Cr(Mn)_xO_y$ oxide, but one can also find here locally isolated $Mn(Fe)_xO_y$ oxides. After 24 h (Figure 12), one observes an outermost oxide of Mn in which Fe, Co and a small quantity of Cr are present; an intermediate oxide of Mn and of Fe with the presence of Cr; and an inner scale of Cr and Mn oxides in similar proportions. This latter oxide scale's constitution remained globally the same until reaching 62 h of exposure (Figure 13).

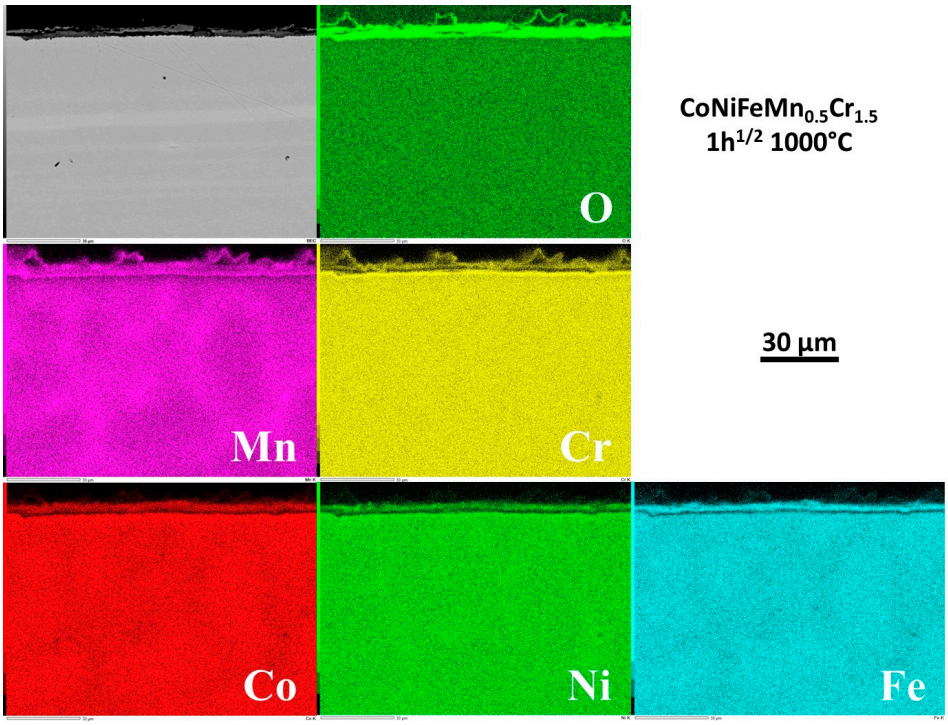

Figure 10. Elemental distribution of the external oxide and in the subsurface after 1 h30 of exposure to air at 1000 °C.

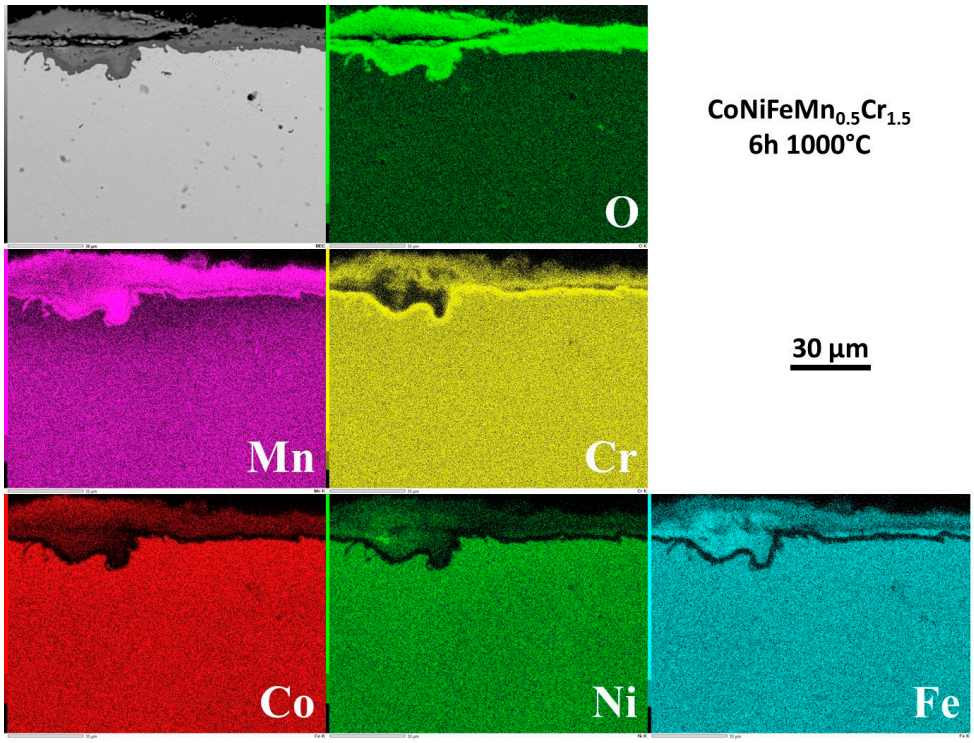

Figure 11. Elemental distribution of the external oxide and in the subsurface after 6 h of exposure to air at 1000 °C.

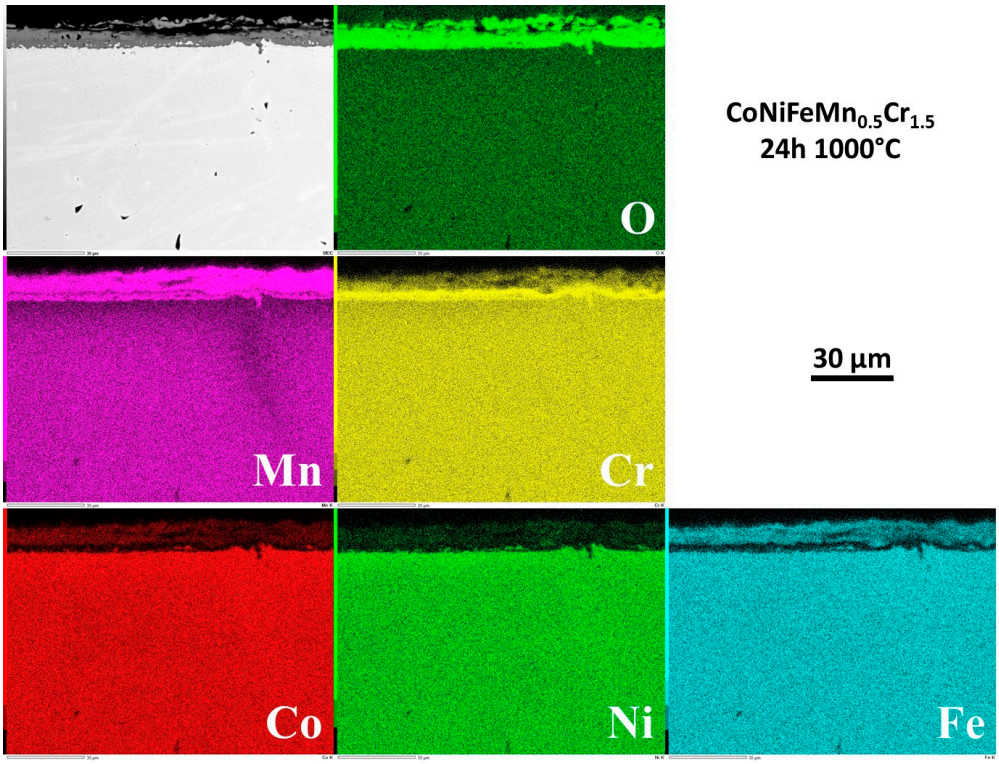

Figure 12. Elemental distribution in the external oxide and in the subsurface after 24 h of exposure to air at 1000 °C.

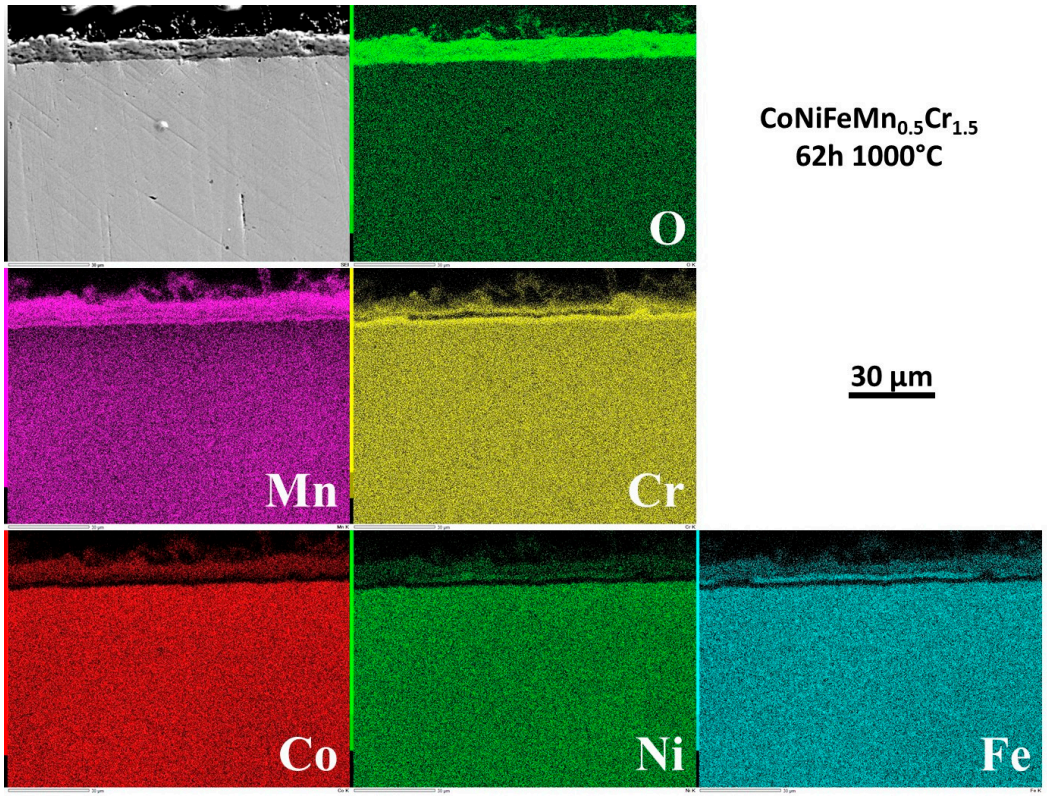

Figure 13. Elemental distribution in the external oxide and in the subsurface after 62 h of exposure to air at 1000 °C.

3.8. Internal Changes in Composition in the Alloy

The analyses of the subsurface show that no internal oxidation occurred (SEM/BSE or EDS elemental maps). However, the chemical composition of the subsurface became increasingly modified by comparison with the initial state of the alloy. Indeed, the alloy became chemically homogenized during the first hours spent at 1000 °C and, after 6 h, the initial Mn-segregated intergranular areas formed at the end of solidification are no longer visible.

However, an impoverishment in both Mn and Cr developed from the interface with the external oxide scale. The Mn- and Cr-depleted depths increased with time. More quantitative information about this chemical evolution in the subsurface can be found in Figure 14, where one can see the progress of the inwards extension of depletion.

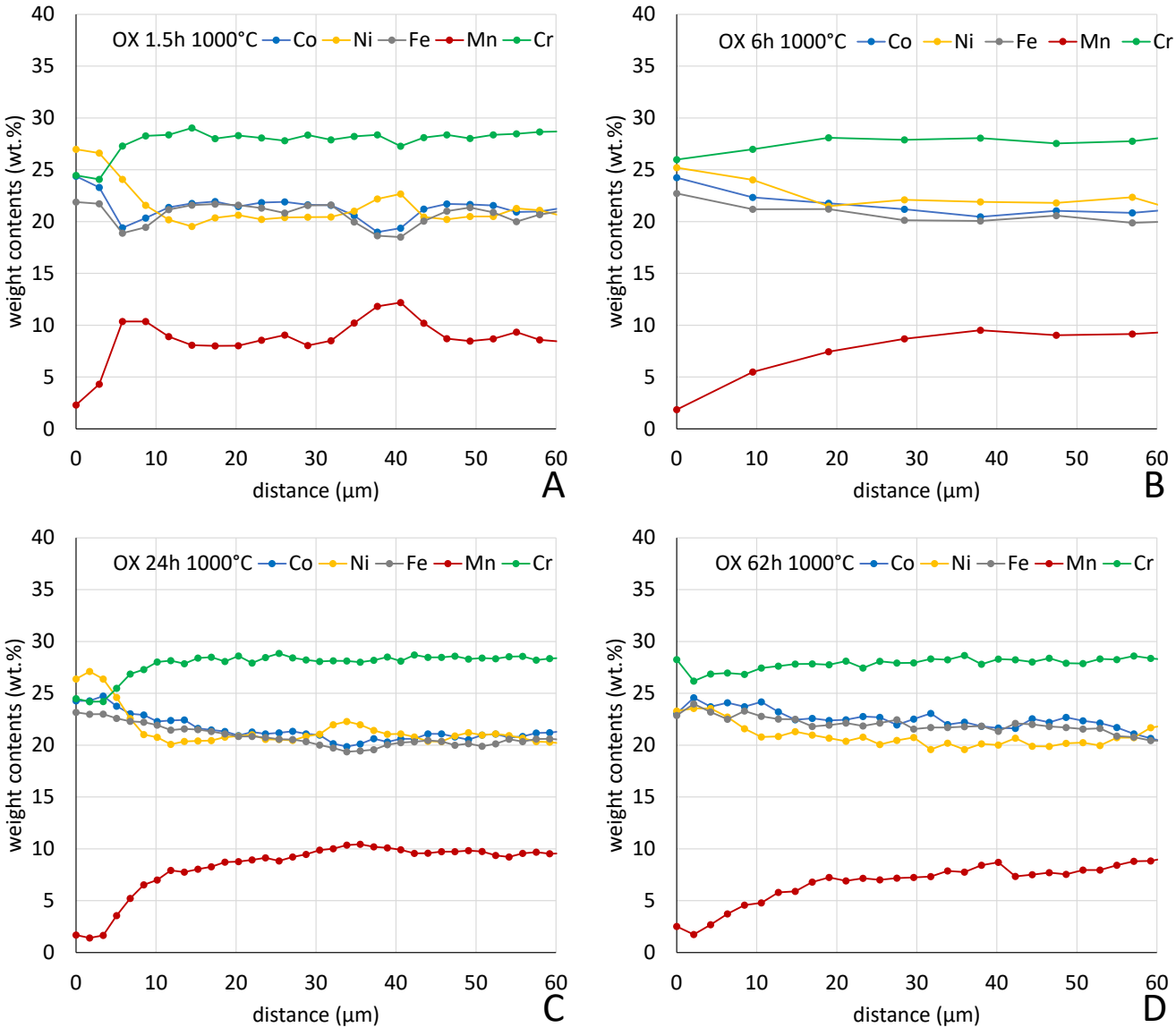

Figure 14. Concentration profiles in the subsurface of the alloys acquired internally from the interface with the external oxide scale.

4. Discussion

Carrying out oxidation tests on a series of alloy samples with interruptions after different durations allowed us to gain a better understanding of how the oxidation products develop, which is not really possible by performing a single thermogravimetry run, as was recently conducted with this alloy [15]. Investigating the composition and structure of oxides formed, step by step, led to the discovery that the multi-constituted oxide scale observed at the end of the long oxidation test in fact existed since the earliest hours of the test: after 1.5 h, Mn-rich oxides, Cr-rich oxides and oxides involving all the elements are all already present as thin layers which will thicken thereafter with time. Without this information, one may imagine other scenarios such as the appearance of an oxide of Co, Ni and Fe after a couple of hours, followed by the formation of chromia and later the formation of manganese oxide after 10 to 20 h. This simultaneous growth of all oxides, all entirely covering the sample surface, explains the possibility of a parabolic kinetic for mass gain, which was previously observed and found again here with seven values. Indeed, if chromia appears solely at the beginning or appears only after several tens of hours, this may lead to different successive regimes and then mass gain kinetics. Here, the mass gain kinetic was parabolic over the whole 62 h, and it was possible to determine the parabolic constant (Kp) at 1000 °C: 6.5×10^{-12} g^2 cm^{-4} s^{-1}. This value, which is consistent with the Kp value recently obtained on the same alloy but using a thermo-balance (6.0×10^{-12} g^2 cm^{-4} s^{-1} in dry 80% N_2-20%O_2 synthetic air [19]), is logically higher than that of a chromia-forming alloy obtained at 1000 °C, such as a Ni-30 wt.% Cr model alloy, for example (2.8×10^{-12} g^2 cm^{-4} s^{-1} [20]). Such a complex mode of development and growth of the external scale does not offer good protection against oxidation, and this explains the higher Kp value as well as the brittleness leading to the loss by parts of the external oxide here and there during handling for surface SEM examination and while preparing the cross-sections (as a consequence, the thicknesses were lower than before metallographic preparation).

The parabolic mass gain and the development of Mn-rich oxides placing chromium in a secondary role in terms of importance, as well as the vulnerability to oxide spallation, were reported earlier by other authors (e.g., by Kai et al. [12] and Kim et al. [14]). The fast diffusion of Mn at high temperature (1000 °C or slightly below) has also been noted (e.g., by Dehury et al. [15]). On the other hand, thanks to the lower Mn presence associated with the greater content in Cr, the kinetic constant determined from the seven mass gain values is significantly lower than for the Cantor's alloy (45×10^{-12} g^2 cm^{-4} s^{-1} [12]), as is the oxide quantity formed.

5. Conclusions

As soon as oxidation starts, all the elements constituting the $CoNiFeMn_{0.5}Cr_{1.5}$ alloy take part in the phenomenon, and the process continues during the following tens of hours. In contrast with chromia-forming alloys, for which several oxides also form initially (including CoO or NiO) but with a rapid switch to chromia only oxides, manganese continues to accompany chromium in the continuation of oxidation. This causes faster oxidation and possible problems of scale spallation due to the bad quality of some of the oxide layers (the one rich in Mn shows presence of pores and small shrinkage defects) by comparison with the compact and adherent innermost chromia-like Cr-rich M_2O_3 oxide. This work will be extended soon to investigate how the development of the oxide scale can be influenced by the choice of other Mn contents in alloys, by the temperature level and by the composition of the gaseous oxidant environment.

Author Contributions: Conceptualization, P.B.; methodology, P.B.; validation, P.B.; formal analysis, L.A. and P.B.; investigation, L.A. and P.B.; resources, P.B.; data curation, P.B.; writing—original draft preparation, P.B.; writing—review and editing, P.B.; visualization, P.B.; supervision, P.B.; project administration, P.B. All authors have read and agreed to the published version of the manuscript.

Funding: This research received no external funding.

Data Availability Statement: The data presented in this study are available in the article.

Acknowledgments: The authors wish to thank Erwan Etienne and Lionel Aranda for their technical help, as well as Romin Chevalme, Yasmina El Hadad and Siouare Hammi, students in the same Master's of Solid Chemistry program as the first author of this article.

Conflicts of Interest: The authors declare no conflicts of interest.

References

1. Sims, C.T.; Hagel, W.C. *The Superalloys*; Wiley-Interscience: New York, NY, USA, 1972.
2. Donachie, M.S.; Donachie, S.J. *Superalloys: A Technical Guide*, 2nd ed.; ASM International: Materials Park, OH, USA, 2002.
3. Ilyas, S.; Ranjan Srivastava, R.; Singh, V.K.; Chi, R.; Kim, H. Recovery of critical metals from spent Li-ion batteries: Sequential leaching, precipitation, and cobalt-nickel separation using Cyphos IL104. *Waste Manag.* **2022**, *154*, 175–186. [CrossRef] [PubMed]
4. Kriese, F.; Lassen, S.; Niemeyer, B. Recovery process for critical metals: Selective adsorption of nickel(II) from cobalt(II) at acidic condition and elevated temperature. *Adsorp. Sci. Technol.* **2023**, *1–2*, 5334353. [CrossRef]
5. Kofstad, P. *High Temperature Corrosion*; Elsevier Applied Science: London, UK, 1988.
6. Young, D.J. *High Temperature Oxidation and Corrosion of Metals*; Elsevier Corrosion Series: Amsterdam, The Netherlands, 2008.
7. Cantor, B. Multicomponent high-entropy Cantor alloys. *Prog. Mater. Sci.* **2021**, *120*, 100754. [CrossRef]
8. Bracq, G.; Laurent-Brocq, M.; Perriere, L.; Pires, R.; Joubert, J.M.; Guillot, I. The fcc solid solution stability in the Co-Cr-Fe-Mn-Ni multi-component system. *Acta Mater.* **2017**, *128*, 327–336. [CrossRef]
9. Kauffmann, A.; Stueber, M.; Leiste, H.; Ulrich, S.; Schlabach, S.; Szabo, D.V.; Seils, S.; Gorr, B.; Chen, H.; Seifert, H.J.; et al. Combinatorial exploration of the high entropy alloy system Co-Cr-Fe-Mn-Ni. *Surf. Coat. Technol.* **2017**, *325*, 174–180. [CrossRef]
10. Teramoto, T.; Yamada, K.; Ito, R.; Tanaka, K. Monocrystalline elastic constants and their temperature dependences for equi-atomic Cr-Mn-Fe-Co-Ni high-entropy alloy with the face-centered cubic structure. *J. Alloys Compd.* **2019**, *777*, 1313–1318. [CrossRef]
11. Ye, Y.F.; Wang, Q.; Lu, J.; Liu, C.T.; Yang, Y. High-entropy alloy: Challenges and prospects. *Mater. Today* **2016**, *19*, 349–362. [CrossRef]
12. Kai, W.; Li, C.C.; Cheng, F.P.; Chu, K.P.; Huang, R.T.; Tsay, L.W.; Kai, J.J. The oxidation behavior of an equimolar FeCoNiCrMn high-entropy alloy at 950 °C in various oxygen-containing atmospheres. *Corros. Sci.* **2016**, *108*, 209–214. [CrossRef]
13. Liu, L.; Wu, S.; Dong, Y.; Lü, S. Effects of alloyed Mn on oxidation behaviour of a Co–Ni–Cr–Fe alloy between 1050 and 1250 °C. *Corros. Sci.* **2016**, *104*, 236–247. [CrossRef]
14. Kim, Y.K.; Joo, Y.A.; Kim, H.S.; Lee, K.A. High temperature oxidation behavior of Cr-Mn-Fe-Co-Ni high entropy alloy. *Intermetallics* **2018**, *98*, 45–53. [CrossRef]
15. Dehury, R.K.; Gautam, A.; Makani, N.H.; Banerjee, R. Experimental investigation on the effect of Cr and Mn in high temperature oxidation of Cantor alloy. *Met. Mater. Int.* **2024**. [CrossRef]
16. Berthod, P. Strengthening against Creep at Elevated Temperature of HEA Alloys of the CoNiFeMnCr Type Using MC-Carbides. In Supplemental Proceedings of the TMS 2023, San Diego, CA, USA, 19–23 March 2023; pp. 1103–1111. [CrossRef]
17. Berthod, P. High Temperature Oxidation of CoNiFeMnCr High Entropy Alloys Reinforced by MC-Carbides. In Proceedings of the TMS 2023, San Diego, CA, USA, 19–23 March 2023; pp. 933–941. [CrossRef]
18. Amrouche, L.; Chevalme, R.; Hammi, S.; El Haddad, Y.; Etienne, E.; Berthod, P. Metallographic follow-up of the oxidation progress with time of cast Cantor alloy at 1000 °C. In Proceedings of the Supplemental Proceedings of the TMS 2025, Las Vegas, NV, USA, 23–27 March 2025. *accepted*.
19. Spaeter, P.; Gay, C.; Chenikha, N.; Medjahdi, G.; Vernière, A.; Rapin, C.; Aranda, L.; Berthod, P. Oxidation Behavior at 1000 °C of Low-Mn High-Cr Cantor's HEA-Based Alloys Strengthened or Not by MC Carbides. *Corros. Mater. Degrad.* **2023**, *4*, 528–541. [CrossRef]
20. Berthod, P. Kinetics of High Temperature Oxidation and Chromia Volatilization for a Binary Ni–Cr Alloy. *Oxid. Met.* **2005**, *64*, 235–252. [CrossRef]

Disclaimer/Publisher's Note: The statements, opinions and data contained in all publications are solely those of the individual author(s) and contributor(s) and not of MDPI and/or the editor(s). MDPI and/or the editor(s) disclaim responsibility for any injury to people or property resulting from any ideas, methods, instructions or products referred to in the content.